Trichogin GA IV Alignment and Oligomerization in Phospholipid Bilayers

Evgeny Salnikov, Marta De zotti, Sara Bobone, Claudia Mazzuca, Jesus Raya, Alvaro S. Siano, Cristina Peggion, Claudio Toniolo, Lorenzo Stella, Burkhard Bechinger

Trichogin GA IV alignment and oligomerization in phospholipid bilayers

Evgeniy S. Salnikov[1], Marta De Zotti[2], Sara Bobone[3], Claudia Mazzuca[3], Jesus Raya[1], Alvaro S. Siano[4]; Cristina Peggion[2], Claudio Toniolo[2], Lorenzo Stella[3], Burkhard Bechinger[1*]

[1]Institute of Chemistry, University of Strasbourg / CNRS, UMR7177, 67070 Strasbourg, France; [2]ICB, Padova Unit, CNR, Department of Chemistry, University of Padova, 35131 Padova, Italy; [3]Department of Chemical Science and Technologies, University or Rome Tor Vergata, 00133 Rome, Italy, [4]Departamento de Química Organica, Facultad de Bioquímica y Ciencias Biologicas, Universidad Nacional del Litoral, Santa Fe, Argentina

* corresponding author: Burkhard Bechinger
Institut de chimie, 4, rue Blaise Pascal, 67070 Strasbourg, France
Tel.: + 33 3 68 85 13 03; E-mail: bechinge@unistra.fr

Keywords: antimicrobial peptide, membrane permeabilization, in planar helical configuration, supported lipid bilayer, solid-state NMR, ATR FTIR spectroscopy

Table of contents text:

The membrane interactions and structure of the natural antimicrobial peptide trichogin GA IV has been investigated by CD-, ATR FTIR- and solid-state NMR spectroscopy. A model emerges where the peptide preferentially aligns parallel to the membrane surface, forming dimeric and tetrameric assemblies at higher concentrations.

ABSTRACT

Trichogin GA IV is a short peptaibol with antimicrobial activity. This uncharged but amphipathic sequence is aligned at the membrane interface and undergoes a transition to an aggregated state that inserts more deeply into the membrane, an assembly which predominates at P/L 1/20. Here, the natural trichogin sequence was prepared and reconstituted into oriented lipid bilayers. The resulting ^{15}N chemical shift is indicative of a well-defined alignment of the peptide parallel to the membrane surface at peptide-to-lipid ratios of 1/120 and 1/20. When the peptide concentration is increased to 1/8 an additional peptide topology is observed indicative of a heterogeneous orientation, with helix alignments ranging from around the magic angle to perfectly in-plane. The topological preference of the trichogin helix for an orientation parallel to the membrane surface is confirmed by ATR FTIR spectroscopy. Furthermore, ^{19}F CODEX experiments were performed on a trichogin sequence carrying ^{19}F-Phe at position 10. The CODEX decay is in agreement with a tetrameric complex, where the ^{19}F sites are about 9 - 9.5 Å apart. Thus, a model emerges where the monomeric peptide aligns along the membrane surface. When the peptide concentration increases, first dimeric and thereafter tetrameric assemblies form, made up from helices oriented predominantly parallel to the membrane surface. Formation of these aggregates correlates with the release of vesicle contents including relatively large molecules.

ABBREVIATIONS

Aib	α–aminoisobutyric acid
ATR FTIR	attenuated total reflection Fourier transform infrared
CODEX	centerband only detection of exchange
CP	cross polarization
EPR	electron paramagnetic resonance
ESI HRMS	high resolution electrospray ionization mass spectrometry
Fmoc	Fluorenylmethoxycarbonyl
FRET	Förster resonance energy transfer
HPLC	high performance liquid chromatography
MAS	magic angle spinning
MS	mass spectrometry
NMR	nuclear magnetic resonance
PC	1,2-diacyl-*sn*-glycero-3-phosphocholine
PELDOR	pulsed electron-electron double resonance
PheCN	*para*-cyanophenylalanine
POPC	1-palmitoyl-2-oleoyl-*sn*-glycero-3-phosphocholine
POPE	1-palmitoyl-2-oleoyl-*sn*-glycero-3-phosphoethanolamine
POPG	1-palmitoyl-2-oleoyl-*sn*-glycero-3-phospho-rac-glycerol
RP-HPLC	reversed phase high performance liquid chromatography
P/L	peptide-to-lipid ratio
TFA	trifluoroacetic acid
TOAC	2,2,6,6-tetramethyl-piperidine-1-oxyl-4-amino-4-carboxylic acid
trichogin	peptide sequences see Table 1

INTRODUCTION

Peptide-based drugs are currently experiencing increasing interest from pharmaceutical companies. Their dimension and biological characteristics place them in between small molecules and proteins, with great advantages over both of them, either in terms of reduced off-target side effects or economic impact [1]. Nonetheless, peptide-based drugs suffer from their poor plasma and enzymatic stability that shortens their half-lives and prevents the possibility for oral administration.

Peptaibols are endowed with antimicrobial and, in some cases, even antitumor activity [2-4]. They are produced by fungi and their sequence ends in an amino alcohol. Thanks to several, non-coded α-amino isobutyric acid (Aib) residues, peptaibols are resistant towards the action of proteolytic enzymes [5] with great potential as orally-available active agents. The peptaibol family comprises peptides going from 21 amino acids (SCH 643432) to just 4 (peptaibolin) [6].

Trichogin GA IV (trichogin, in brief) is a decamer peptaibol (Table 1), produced by the fungus *Trichoderma longibrachiatum*, being one of the shortest sequences [7]. The trichogin sequence ends in an amino alcohol, and its N-terminus is derivatized with an *n*-octanoyl group, thus extending its hydrophobic character. Trichogin also proved to be a versatile template to build a series of analogs with selective cytotoxic and antimicrobial activity [6,8]. The peptide has low hemolytic activity and possesses a very selective bioactivity [9]. It was reported to be active against several methicillin-resistant strains of *Staphylococcus aureus*, but it is completely inactive against both fungal pathogens and Gram-negative bacteria [5]. Potent antitumor activity of trichogin against several cell lines was also described [9].

The best characterized member of the peptaibol family (and the first to be identified, in 1967) is alamethicin [10]. The membrane interactions of alamethicin were early on investigated by a large variety of biophysical techniques [11, 12] including its topology and oligomerization by solid-state NMR and EPR spectroscopies [13-18]. These studies conclusively demonstrated that alamethicin binds to the membrane and can populate different orientations [19-21]. When the membrane-bound peptide concentration is sufficiently high and/or a transbilayer potential is applied, alamethicin adopts a transmembrane orientation and aggregates in a cylindrical superstructure, like the staves in a barrel, with the more hydrophilic side of the helices facing the water-filled channel lumen [22, 23]. Interestingly, an in-planar topology of alamethicin is stabilized in POPE/POPG membranes [19] indicating that the in-plane to transmembrane equilibrium is governed by a multitude of

factors such as peptide-to-lipid ratio, hydration [24] and lipid composition [19]. In this context it is interesting to note that zervamicin II and ampullosporin A, 15- and 14-amino acid peptaibols, respectively, are oriented parallel to the surface of most phosphatidylcholine (PC) membranes while transmembrane alignments have been observed in PC bilayers made from short C10 or C12 fatty acyl chains [15, 17].

Considering the closely related amino acid composition and physico-chemical properties of all members of the peptaibol family, it is conceivable that they could form pores in a similar way. However, alamethicin comprises 19 amino acids and its helix has a length corresponding almost exactly to the thickness of biological membranes. By contrast, shorter peptaibols (like trichogin) cannot span the whole bilayer in a transmembrane orientation, unless significant modifications of the membrane thickness take place [15, 17]. For this reason, since the isolation of trichogin from *Trichoderma longibrachiatum* [25], multiple research efforts have been devoted to understand its mechanism of pore formation using techniques including NMR [25, 26], EPR [27-30], fluorescence [31-35], X-ray crystallography [36], scanning probe microscopy [37], neutron reflectivity [38], electrochemistry [39-41], and molecular dynamics simulations [38, 42]. Trichogin is known to adopt a mixed 3_{10}-/α-helical conformation under a variety of experimental conditions, mainly thanks to the presence of three helix-inducing Aib residues in its sequence [8, 9, 32, 36]. The helical structure correlates with the peptide's bioactivity, since replacing one of those quaternary residues by Leu, the helical conformation is destabilized when at the same time a much reduced bioactivity is observed [43].

When trichogin-induced leakage of ions from liposomes was investigated, the peptide concentration dependence suggested that 3-4 trichogin molecules are involved in pore formation [44]. Peptide induced leakage was dependent on the sign and value of the transmembrane potential, being activated by cis-positive, but not by cis-negative potentials. Notably, trichogin was about 200 times less active than the longer peptaibol zervamicin. Whereas this low activity and the low molecularity [40, 41, 44] argue against the formation of well-defined pores, ion selective and voltage dependent leakage are in favor of such models.

Trichogin-induced membrane leakage has also been characterized by following the release of the fluorescent dye carboxyfluorescein [25, 35, 38, 45].These data demonstrated that trichogin is able to cause the leakage of relatively large organic molecules, and indeed even leakage of dextran polymers (<MW>=10kDa) has been observed [32]. An interesting observation is that trichogin-induced leakage is strongly dependent on membrane thickness. In liposomes with a hydrophobic thickness comparable to that of biological membranes, trichogin is about 30 times less effective than alamethicin. By contrast, the two peptides

become similarly active in membranes with a thickness comparable to the size of trichogin [38]. A much lower pore forming activity of trichogin, compared to alamethicin, was reported also in natural cell membranes [46].

Many of the previous investigations have been performed with trichogin variants modified at their termini for easier synthesis, by addition of electron spin labels or fluorophores required for the corresponding biophysical investigations. Here, in a first set of experiments the topology of the peptide was investigated by static oriented ^{15}N solid-state NMR on trichogin GA IV where a single natural abundance ^{14}N isotope of a glycine was replaced by ^{15}N, a minor modification not affecting the physico-chemical character of the peptide sequence. When reconstituted into liquid crystalline lipid bilayers that are uniaxially aligned with their normal parallel to the magnetic field of the NMR spectrometer the ^{15}N chemical shift is a direct indicator of the approximate tilt angle relative to the membrane surface [47]. The ^{15}N chemical shift spectra were recorded and analyzed at different peptide-to-lipid ratios. Complementary topological information was obtained by ATR FTIR spectroscopy on supported lipid bilayers [48, 49].

In a second series of experiments, the Ile10 position was replaced by ^{19}F-Phe10 in order to perform the so called centerband only detection of exchange (CODEX) solid-state NMR experiment. Under fast magic angle spinning (MAS) the experiment was initially designed to reveal the correlation times and motional regimes at ambient temperatures [50]. However, when such motions are frozen at low temperatures the CODEX technique allows one to elucidate the aggregated structure through distances in the range of up to 15 Å between specifically ^{19}F-labelled residues [18, 51, 52]. Furthermore, the experiment reveals the number of subunits in the aggregate structure.

Experimental section moved to end → reference update of numbering

Table 1. Trichogin and other peptaibol sequences investigated and discussed in this paper[a]

*n*Oct-Aib-Gly-Leu-Aib-Gly-Gly-Leu-Aib-Gly-Ile-Lol	trichogin GA IV
*n*Oct-Aib-Gly-Leu-Aib-Gly-Gly-Leu-Aib-Gly-Ile-Leu-OMe	trichogin GA IV-OMe
*n*Oct-Aib-Gly-Leu-Aib-Gly-Gly-Leu-Aib-Gly-(^{19}F)Phe-Lol	[^{19}F-Phe10]-trichogin GA IV
*n*Oct-Aib-(^{15}N)Gly-Leu-Aib-Gly-Gly-Leu-Aib-Gly-Ile-Lol	[^{15}N-Gly2]-trichogin GA IV
*n*Oct-PheCN-Gly-Leu-Aib-Gly-Gly-Leu-Aib-Gly-Ile-Lol	[PheCN1]-trichogin GA IV
*n*Oct-Aib-Gly-Leu-Aib-Gly-Gly-Leu-PheCN-Gly-Ile-Lol	[PheCN8]-trichogin GA IV
Ac-Trp-Ala-Aib-Aib-Leu-Aib-Gln-Aib-Aib-Aib-Gln-Leu-Aib-Gln-Lol	ampullosporin A
Ac-Trp-Ile-Gln-Iva-Ile-Thr-Aib-Leu-Aib-Hyp-Gln-Aib-Hyp-Aib-Pro-Phl	zervamicin IIB

Ac-Aib-Pro-Aib-Ala-Aib-Aib-Gln-Aib-Val-Aib-Gly-Leu-Aib-Pro-Val-Aib-Aib-Gln-Gln-Phl	alamethicin (F50/7)

[a] *n*Oct, n-octanoyl; Lol, leucinol; Aib, α-aminoisobutyric acid; Iva, isovaline; Hyp, *trans*-4-hydroxyproline; Phl, phenylalaninol; Ac-, acetyl.

RESULTS

Peptides were prepared with good yield and purity including selectively labelled sequences for solid-state NMR spectroscopy. Whereas the incorporation of ^{15}N isotopic labels allows for the investigation of the peptide alignment relative to the membrane surface, ^{19}F has been included for distance and oligomerization measurements by CODEX MAS experiments.

In order to investigate its membrane interactions in more detail, [^{15}N-Gly2]-trichogin GA IV was reconstituted into uniaxially oriented POPC membranes and inserted into the receiver coil of the NMR probe with the sample normal parallel to the magnetic field direction. In this configuration the ^{15}N chemical shift is a direct indicator of the approximate tilt angle of helical peptides [47]. Whereas chemical shifts around 200 ppm are characteristic of transmembrane helices, peptides that are oriented parallel to the membrane surface exhibit ^{15}N chemical shifts < 100 ppm. Notably, the ^{15}N solid-state NMR approach is a non-invasive method to angular information of the labelled ^{15}N-H vector(s) relative to the external magnetic field of the NMR spectrometer (and in the case of uniaxially aligned samples also the membrane normal). The spectral line shapes, intensities and chemical shift positions are also indicative if the labelled site is part of a structured helix interacting with the oriented lipid membrane (Fig. S1A,B). However, the technique does not provide information about the depth of penetration of the peptides into the membrane.

When [^{15}N-Gly2]-trichogin GA IV is investigated at P/L of 1/120 or at P/L 1/20 a single sharp resonance at 79±2 ppm is observed clearly indicating that the peptide exhibits a uniform alignment close to parallel to the bilayer surface (Figs. 1A,C and S2). In the spectrum obtained at P/L 1/20 (Fig.1C) additional signal intensities were also observed in the 110 ppm region, which were only 5%-10% of the integral intensity. We tentatively assign this contribution to peptide oligomers that interact only weakly with the membrane thus undergoing isotropic motions (Fig. S1C) [32].

When a more concentrated sample was investigated at P/L 1/8 two signal intensities become obvious (Fig. 1E). The sharp resonance at 79 ppm was accompanied by a broader distribution of signal intensities reaching from 50 to 115 ppm with a maximum at 62 ppm.

At 250 K the spectrum of this sample (P/L 1/8) was characterized by a distribution of ^{15}N signals ranging from 45ppm to 135ppm (Fig. 1G).

When the ^{31}P NMR spectra of the three samples were investigated, a predominant intensity was observed at 28 ppm with much smaller intensities reaching up to -16 ppm (Fig. 1B,D,F), indicating that the phospholipid is in a liquid crystalline state and the bilayers are well oriented [53, 54]. Interestingly, in contrast to the large increase in signal intensities < 30 ppm that occur when the peptide-lipid-ratio of amphipathic cationic antimicrobial sequences is increased > 1/50 [55-57], in the presence of trichogin closely related ^{31}P NMR line shapes are observed for all three peptide-to-lipid ratios (Fig. 1B,D,F). Overall, even at the high peptide concentrations, the peptide and lipids aligned well, thereby resembling the behavior of alamethicin [17]. Due to lack of charged amino acids or of tryptophans, that tend to form anchors at the membrane interface [58], these hydrophobic sequences can insert more deeply into the membrane interior. Thereby, in contrast to cationic amphipathic antimicrobial peptides, peptaibols (*see* Fig. S3), including trichogin, have been shown to have little disordering effect at the membrane interior [42, 59].

In Figure 1E the narrow signal and the contributions from the broad distribution of alignments are well separated indicating that the two populations are in slow exchange at the time scale of the ^{15}N chemical shift anisotropy (10^{-4} sec). By comparison to previous investigations [27, 28, 32-34, 60], we assign the sharp resonance at 79 ppm to monomeric trichogin aligned parallel to the membrane surface (Fig. 1A,C,E) whereas the broad contribution is from membrane inserted oligomers that co-exists at the high peptide-to-lipid ratio (Fig. 1E). At 250 K the POPC bilayer is in the gel state (T_c = 271 K for pure POPC) and the ^{15}N solid-state NMR spectrum suggest that the oligomeric arrangement of the peptides is favored under this condition (Fig. 1G). The ^{15}N solid-state NMR spectra of the oligomers are indicative of a distribution of alignments where the orientation relative to the magnetic field of the NH vector and thus the tilt angle of the helix long axis reaches from about 50° up to parallel to the membrane surface (i.e. 90°, Figs. 1E,G, S1B).

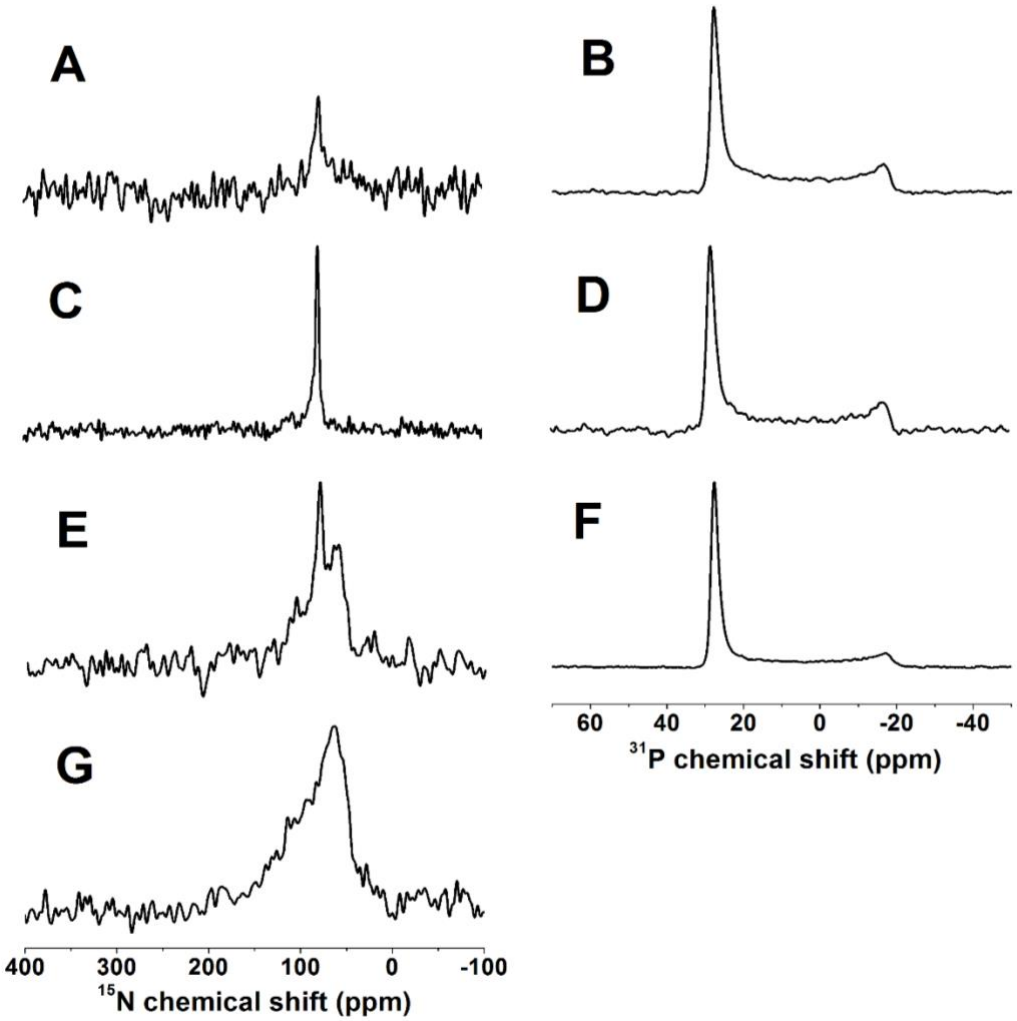

Figure 1. Proton-decoupled ^{15}N- (A,C,E,G) and ^{31}P- (B,D,F) solid-state NMR spectra of [^{15}N-Gly2]-trichogin in POPC membranes oriented with the sample normal parallel to the magnetic field direction at concentrations of 0.8 mole% (P/L=1/120, panels A and B), 5 mole% (P/L=1/20, panels C and D) and 11 mole% (P/L=1/8, panels E-G). Spectra A-F were measured at 295K, while for panel G the temperature was set to 250 K. The exponential line-broadening applied before Fourier transformation is 50 Hz for A and C and 200 Hz for E and G.

These findings were confirmed by polarized ATR-FTIR spectroscopy, which allows the determination of the average orientation of helical peptides inside lipid bilayers (Figure 2, Table 2). For these studies, we employed an unlabeled trichogin analog and two sequences labeled with PheCN, which had been previously investigated by exploiting the PheCN fluorescence and IR signals,[61] demonstrating insertion in the membrane [62]. Table 2 reports the dichroic ratio (R) for the amide I band in the region between 1600 and 1700 cm^{-1}, the order parameter (S), and the angle formed by the helix axis with the bilayer normal α [21]. For all analogues an average angle of about 60-80° was determined. This value could

correspond to an average of different orientations populated by the peptide in the membrane, or it could correspond to a tilted arrangement. The orientation did not change significantly with P/L (Table 2). Incidentally, the position of the amide I peak was between 1653 and 1658 cm^{-1} for all analogs and experimental conditions, confirming the attainment of a helical conformation in the bilayer [63]. Helical conformations of trichogin in the presence of liposomes are also observed by CD spectroscopy (Figure S4).

Table 2. ATR-FTIR analysis of trichogin GA IV modified with PheCN at position 1 or 8, or with a C-terminal methyl ester, in a POPC membrane. Values of dichroic ratio (R), order parameter (S), cosine squared and angle between the peptide helix and the normal to the lipid bilayer are listed.

Analog	Peptide/lipid	R	S	$\cos^2(\alpha)$	α (deg)
[PheCN1]-trichogin GA IV	1:40	1.6	-0.13	0.21	60
[PheCN1]-trichogin GA IV	1:10	1.5	-0.17	0.17	70
[PheCN8]-trichogin GA IV	1:40	1.6	-0.13	0.21	60
[PheCN8]-trichogin GA IV	1:10	1.6	-0.13	0.21	60
Trichogin GA IV-OMe	1:20	1.2	-0.30	0.04	80

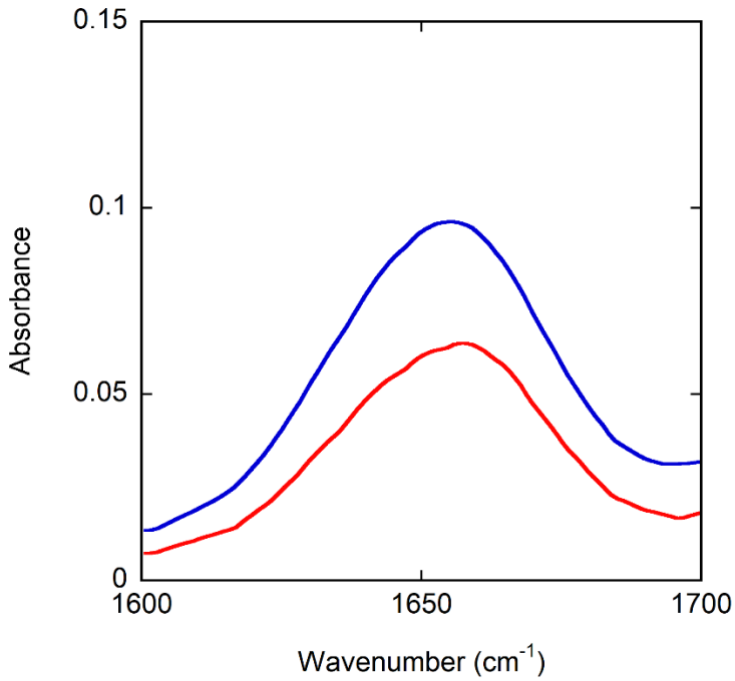

Figure 2. Representative polarized ATR FTIR spectra of the amide I band with the polarizer oriented at 0° (blue) and 90° (red) for [PheCN1]-trichogin GA IV at a peptide-to-lipid ratio of 1/10.

Next, we investigated in more detail the oligomeric structure of trichogin when inserted into lipid bilayers. To this end, ^{19}F-Phe10-trichogin was reconstituted into POPC bilayers and studied by ^{19}F MAS solid-state NMR spectroscopy. The ^{19}F CODEX experiments allow one to count the ^{19}F spins that are interacting within a radius of 15 Å, to measure the dipolar interactions and thereby the distances between these nuclei [18, 51, 52]. The experiment drives the exchange of magnetization due to dipolar interactions, where the signal under mixing conditions S relative to the corresponding signal without exchange S_0 is recorded as a function of the mixing time. The signal diminishes under spin exchange conditions thus that at long mixing times the initial magnetization is equally distributed among the differently positioned molecules in the cluster. This effect reduces the CODEX echo intensity to 1/N (where N is the number of magnetically nonequivalent ^{19}F-nuclear spins per aggregate).

The analysis of such data requires good knowledge of the overlap integral F(0) which is also affected by the dynamics of the side chain. Freezing the sample to 240 K much suppresses conformational exchange, but rotations and flipping motions around bonds still persist even when the sample is frozen. Therefore, we first calibrated the F(0) value of the ^{19}F-Phe side chain for structural analysis by CODEX using 4-^{19}F-2′-nitroacetanilide (Figure 3) under the same experimental conditions also used for the investigations of trichogin in membranes (Figure 4). Fig. 3A shows the experimental ^{19}F solid state NMR spectra for S (at a 200 ms mixing time), for S_0 (no mixing) and the corresponding CODEX curve (S/S_0 as a function of mixing time). Furthermore, the known distance between the ^{19}F in the 4-^{19}F-2′-nitroacetanilide microcrystals is used to simulate CODEX curves to adjust the overlap integral under the conditions of the trichogin experiments (Fig. 3B). 4-^{19}F-2′-nitroacetanilide has a long r_{ij}^{nn} of 11.5 Å, where the second moment exceeds the nearest neighbor ω_{ij}^2 by a factor of 43, making the effective coupling equivalent to an r_{ij}^{nn} of 6.1 Å rather than 11.5 Å. Finally the quality of the data fits is analyzed as a function of F(0) (Fig. 3C).

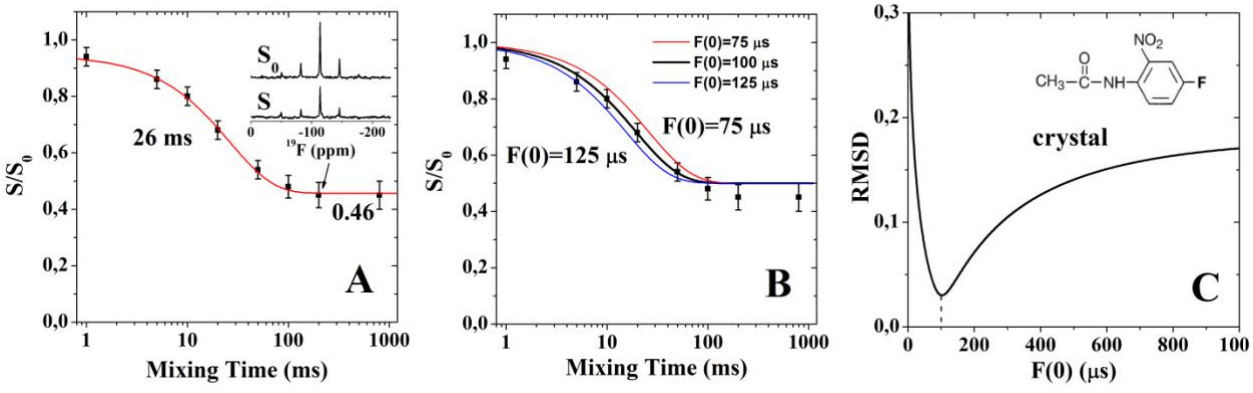

Figure 3. CODEX curve of a 4-^{19}F-2′-nitroacetanilide powder (MAS 15 kHz, 240K). **A.** The experimental data are compared to an exponential fit with decay time of 26 ms and a plateau value at 0.46 (red solid line). The insert shows the experimental ^{19}F solid state NMR spectra at 200 ms mixing time (S) and in the absence of mixing (S_0) **B.** Simulation of the CODEX exchange with spin dimers at the effective distance of 6.1 Å is demonstrated for the 3 different F(0) values. **C.** The quality of the fit is plotted as a function of F(0) with a minimum observed at F(0) = 100 µs.

The CODEX experiment using [^{19}F-Phe10]-trichogin GA IV in POPC bilayers at a peptide-to-lipid ratio of 1/8 is shown in Fig. 4A. The signal S when compared to the intensity at zero mixing time, S_0, reaches a plateau at around ¼ which suggests that four peptides form an oligomeric structure. Furthermore, the signal can be described by a mono-exponential decay with a characteristic time constant of 160 ms, characteristic of a nearest distance of 9 - 9.5 Å between the fluorinated sites of the monomers (Fig. 4B). The geometric arrangement and the distances that govern such a decay are also shown in Fig. 4B.

A plateau of ¼ for S/S_0 can also be obtained from linear combinations of other oligomeric structures (see analysis of data obtained earlier on for alamethicin, in SI of reference 18). For example, a combination of 10% monomer and 90% hexamer could also result in a plateau of 0.25. Notably, for a predominantly tetrameric arrangement the statistical probability to also have inter-oligomeric contacts between tetramers affecting the CODEX decay curve is rather small and can be ignored (see SI of reference 18). The exact distance between monomers is not only dependent on the statistical errors (as indicated by the bars in Fig. 4) but also on the accuracy of the determination of F(0) which makes the calibration shown in Figure 3 so important.

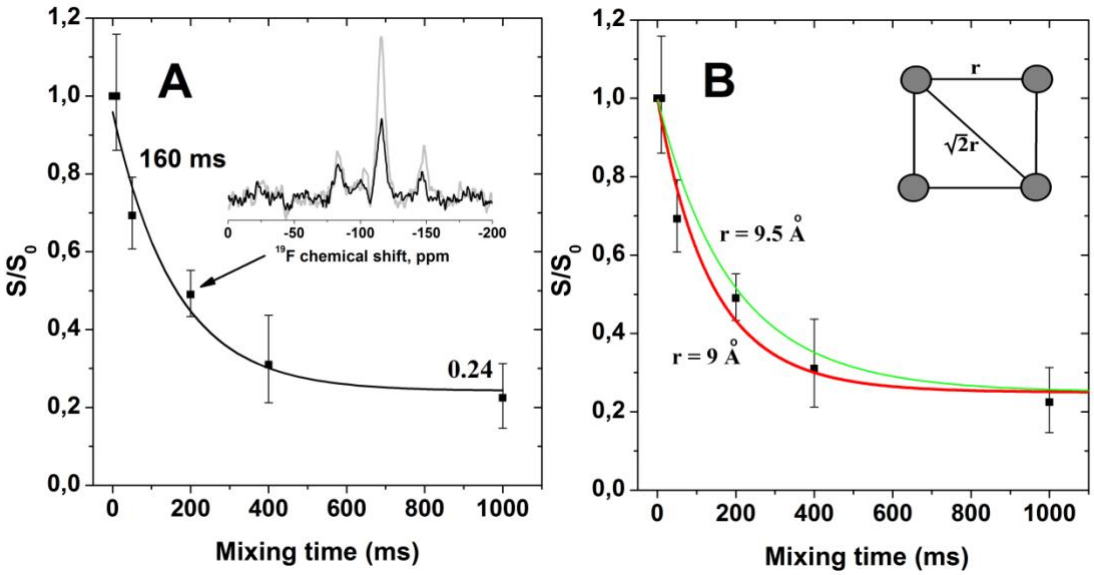

Figure 4. CODEX curve of [^{19}F-Phe10]-trichogin GA IV in POPC at P/L=1/8 (MAS 15 kHz 240K). A fit with exponential decay is shown in panel A. The ^{19}F spectra of S and S_0 for the mixing time of 200 ms are shown in the inset in panel A. The best fit with a tetramer geometry is shown in panel B with the red curve representing a nearest distance between spins of 9 Å and the thin green curve a nearest distance between spins of 9.5 Å.

DISCUSSION

Membrane insertion and oligomerization as a function of P/L

The solid-state NMR data are suggestive that an equilibrium between monomeric (at low P/L) and tetrameric peptide at high P/L (or of similar oligomer size) governs the trichogin structure in POPC lipid bilayers. Indeed, previous EPR and fluorescence spectroscopy investigations have identified several possible supramolecular membrane assemblies. At P/L <1/100 an in-plane alignment of trichogin monomers has been identified by a number of investigations [27, 30, 32-34]. At P/L of about 1/20 the formation of small oligomers/dimers has been observed accompanied by a change in membrane topology and trichogin dynamics [27, 28, 32-34, 60]. Upon further increasing the peptide concentration, higher order oligomers have been observed (Fig 4) [64]. Equilibria connecting different topological and association states have also been observed for other AMPs, where hydration, membrane phase, lipid composition, membrane thickness and the presence of other peptides all have been shown to be important [15, 19, 24, 65-67].

Monomeric surface-bound state at P/L 1/120

Here, for the first time the peptide alignment at P/L below the threshold value for peptide aggregation and insertion (≤1/20)[32-34] has been investigated in a liquid crystalline bilayer using a non-invasive ^{15}N and ^{31}P solid-state NMR approach (Fig. 1). The data are indicative of a well-defined alignment of the trichogin helix parallel to the membrane surface (Figs. 1 and S1) which is in good agreement with previous investigations using TOAC nitroxide -labelled trichogin and EPR spectroscopy in PC membranes [27, 29, 30, 68] or of fluorophore-labelled trichogin [32-34]. The fluorescence spectroscopy investigation also showed a location of the fluorophores at about 1 nm from the bilayer center. EPR investigations where the positioning of the TOAC labelled sites was found at the level of fatty acyl chain position 9-11 agree with these findings [27]. FRET experiments between the fluorescent analogues and labeled lipids demonstrated that trichogin is able to distribute between both membrane leaflets even before forming pores [33]. The interfacial alignment also agrees with the amphipathic character of the peptide sequence [68]. In-planar helix alignments have previously also been observed for a multitude of charged [55, 65, 69-72] and uncharged amphipathic sequences [67].

Membrane insertion above the P/L threshold

Time-resolved fluorescence and FRET measurements have demonstrated that the peptides aggregate both in water (in the µM range) and in the membrane [32]. A correlation was observed between membrane-perturbing activity and aggregate formation in the membrane and between the fraction of aggregated and inserted peptide. Above a threshold peptide-to-lipid ratio trichogin has been shown to aggregate and to insert more deeply into the membrane [27, 30, 32-34, 60]. Notably, the ^{31}P solid-state NMR data (Fig. 1B,D,F) are indicative of well-oriented PC bilayers even in the presence of high trichogin concentrations. This observation is suggestive of less-disruptive membrane interactions probably by a deeper insertion into the membrane when compared to cationic amphiphiles. The present finding is in agreement with previous measurements of peptaibols in liquid crystalline bilayers even in the presence of hydrophobic mismatch and/or when the peptides adopted in-planar alignments (Fig. S3) [15-17, 19]. In addition, in the case of the trichogin GAIV-OMe, fluorescence anisotropy experiments on a membrane embedded fluorophore ruled out significant perturbation of membrane order and dynamics even at P/L=1:8, both for fluid and gel phase bilayers [42]. These data suggest that the inserted, aggregated species is responsible for membrane leakage possibly by defects along the lipid -peptide interface. In view of these correlations the oligomeric state is of particular interest and its structure has

been studied in further detail here (Figs. 1E,G and 4) and in previous EPR and fluorescence spectroscopy investigations [27, 30, 32, 60].

Structure of the complex observed in the absence of a transmembrane voltage

Upon increase of the P/L above the threshold value (i.e. at about 1/30 to 1/20)[32-34] EPR ESEEM data are indicative that the N-terminus moves deeper into the membrane whereas positions 4 and 8 remain about the same [27]. The deeper insertion of position 1 can be explained by a change in tilt angle or of rotational pitch, or both. The ^{15}N solid-state chemical shift does not vary when increasing the peptide-to-lipid ratio from 1/120 to 1/20 indicating no major changes in tilt angle (Fig. 1A,C). It is thus probable that the predominant topological changes are due to a rotation along the helix long axis upon dimerization which would also agree with a change in water exposure of the N-terminus but not of positions 4 and 8 [27, 29]. Notably, whereas a recent investigation confirmed an in-planar alignment in eggPC membranes at P/L ≤1/20, a localization of the N-terminus next to deuterated isopropyl group of cholesterol has been observed in eggPC/cholesterol 1/1 membranes thereby emphasizing the importance of membrane lipid composition for the topology of trichogin [28, 29]. PELDOR investigations at P/L 1/20 are indicative of dimeric contacts between labelled N-termini that range from 1.5 to 4 nm with a maximum at 2.5 nm [27] and the appearance of an additional peptide population undergoing a slow motional regime [60].

At even higher P/L (1/8) another peptide population appears (Fig. 1 E,G). The ^{15}N solid-state spectra are characterized by two populations in slow exchange one corresponding to the topologies observed at lower P/L and a second one which is characterized by a wide distribution of alignments ranging from tilts along the magic angle to in-planar orientations (Fig. S1). The corresponding CODEX experiments are indicative of association of four peptides into a structure with intermolecular distances of 9-9.5 Å and 12.8 Å (corresponding to 9 Å *√2; Fig. 4B). Notably, from ion leakage experiments a dependence of leakage rate on peptide concentration also pointed to 3-4 trichogin molecules being involved in the rate limiting step [44]. Tetramers formed by two trichogin dimers were also observed in apolar solutions using PELDOR spectroscopy, which dissociated in more polar environments. The intermolecular dipolar couplings between TOAC labels at the first or fourth position were in the range of 20-25 Å [73, 74].

Neutron reflectivity experiments demonstrated that the bilayer thickness decreases when the peptide concentration is increased above a membrane bound peptide-to-lipid ratio of 1/20 [38]. This finding was originally interpreted as due to a transition to a transmembrane

orientation, but it may be caused by membrane adaptation to the insertion of the trichogin aggregates. At the same time, in contrast to cationic amphipathic peptides [53, 56, 57], the global orientational order of the bilayer and the order at the level of the phospholipid head groups remain largely unaffected by trichogin in the range P/L 1/120 to 1/8 (Fig. 1B,D,F).

Models for the membrane-associated monomer, dimer and tetramer

Whereas the structural information is insufficient to establish an atomistic model of the arrangement of the trichogin helices, some geometrical considerations are of interest. The ^{15}N solid-state NMR data indicate that up to 1/20 the helices are oriented parallel to the membrane surface. This situation is schematically illustrated in Figure 5A.

When a threshold concentration of about 1/50 is reached, dimerization and a deeper penetration of the peptide inside the membrane has been observed by EPR and fluorescence spectroscopies [27, 30, 32-34, 60]. The ^{15}N solid-state NMR spectra remain unchanged suggesting that the membrane topology is unaltered between P/L 1/120 and 1/20 (Fig. 4A, C). It is also possible that small changes of the tilt angle are accompanied by alterations of the rotational pitch such that the same ^{15}N chemical shift spectrum is observed in the oriented samples (Fig. S2). Notably the global lipid orientational order is hardly affected even by the highest peptide concentrations (Fig. 1B,D,F). It is also possible that dimerization and deeper membrane penetration of some of the labels is dependent on the peptide-to-lipid ratio, the lipid composition [29, 75], the detailed trichogin sequence including terminal modifications [76], TOAC replacements or fluorophore additions. Fig. 5B shows an antiparallel dimer with an N-N intradimer distance of about 25 Å corresponding to the most populated conformers from PELDOR experiments [27]. These data are characterized by a large range of dipolar couplings covering 15 to 40 Å. Thus, it is possible that the dimeric structure is highly heterogenous. Alternatively, distances within this range are also obtained when dimers are positioned in opposite leaflets of the bilayer (Fig. 5B). Considering the accumulation of Aib, Leu and Gly residues along well-defined faces of the peptide helix (see helical wheel representation in reference 30) a Leu-zipper arrangement or GxxxG motifs in a hydrophobic environment [77] could be involved in stabilizing the dimer.

Finally, at even higher P/L of 1/8 the CODEX experiments reveal a tetrameric structure with a distance between the ^{19}F-Phe10 sites of about 9-9.5 Å (Fig. 4). The alignment of helices from oriented ^{15}N solid-state NMR spectra remains predominantly in-planar albeit a large range of topologies is observed (Fig. 1G). Fig. 5C schematically shows a tetramer made up of two dimers.

When compared to other peptaibols it is interesting to note that whereas for the ten-residue trichogin an in-planar alignment predominates (Figs. 4 and 5), the 15-residue zervamycin II or ampullosporin A peptaibols exhibit in-planar alignment in membranes of average hydrophobic thickness but transmembrane alignments in thin membranes [15, 17]. Even the 19-residue alamethicin which is considered the paradigm of transmembrane helical bundle formation [38, 42], in-planar alignment has been observed at low concentration or in POPE/POPG 3/1 bilayers which are considered good mimetics for bacterial membranes [15, 19, 24].

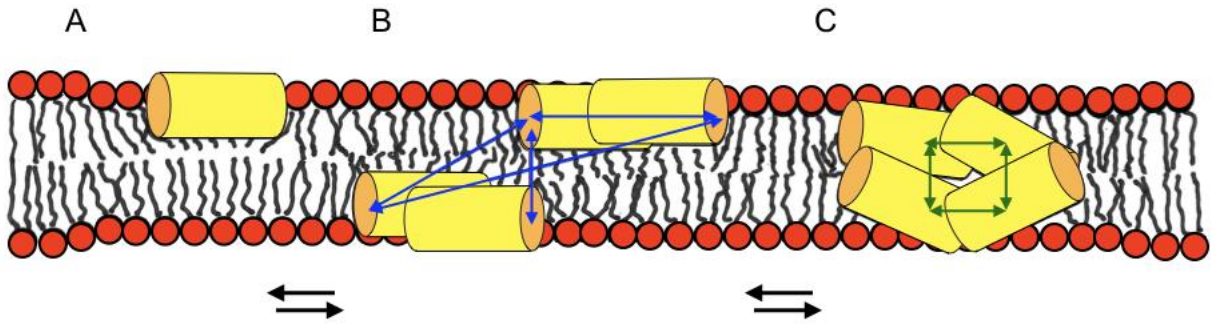

Figure 5. Schematic model of the interactions of trichogin GA IV with POPC bilayers at peptide-to-lipid rations of **A** ≤ 1/100, **B** 1/20 and **C** 1/8. The blue arrows indicate the range of PELDOR distances of 15-40 Å measured in the dimer [27] and the green arrows highlight four ≈ 9-10 Å distances that agree with the CODEX experiment shown in Fig 4.

Fig. 5 summarizes different states that have been described in biophysical experiments. The transitions depend on the detailed experimental conditions and can be influenced by subtle changes in the peptide sequence. Therefore, the non-invasive nature of the ^{15}N isotopic labelling and the topological analysis of the peptide sequence in the liquid crystalline bilayers used here (Figs. 1 and 2) are of particular value, while the investigation of the peptide aggregation state at high P/L provides additional insight into the mechanism of action of this short antimicrobial peptide (Fig. 4).

It should also be mentioned that the possibility exists that a fraction of peptide exists with different topology, which remains hidden in the noise of the ^{15}N solid-state NMR spectra. In this case the in-plane oriented peptide could be the energetically favored but not the most active state. Whereas the design and investigation of histidine-containing model peptides showed that cationic peptides are indeed powerful antimicrobials when oriented parallel to the membrane surface the question remains if this is also the most active state for the short, neutral peptaibols. In the presence of transmembrane electric voltages further

changes of the trichogin topological state can be envisioned [40, 41, 44], due to the interaction of the helix dipole moment with the external electric field [78].

However, membrane passage of rather bulky molecules has been observed in fluorophore release experiments in the absence of transmembrane electric fields [25, 32, 38, 45] which is indicative of helical bundles of considerable dimensions [11] or of membrane perturbations involving supramolecular peptide - lipid arrangements [7, 79] such as those shown in Fig. 5B and C [80]. Thus the shorter peptaibols align preferentially parallel the membrane surface, as observed for cationic amphipathic peptides [80]. At high peptide concentrations trichogin oligomers penetrate deeper into the membrane core whereas the cationic peptides have a strong effect on membrane integrity.

MATERIALS AND METHODS

Peptide Synthesis

The trichogin GA IV sequences investigated in this paper are shown in Table 1. ^{15}N-trichogin was obtained by solid-phase peptide synthesis following the general procedure described in reference 8. Fmoc-protected ^{15}N-Gly was synthesized and incorporated into the sequence at position 2. The peptide was cleaved from the resin by repeated treatments with 30% 1,1,1,3,3,3-hexafluoroisopropanol in dichloromethane, purified by preparative reversed phase (RP)-HPLC on a Phenomenex C18 column (40 × 250 mm, 10 μ, 300 Å) using a Shimadzu (Kyoto, Japan) system (flow rate 15 ml min^{-1}, λ = 206 nm). Eluant A, H_2O + 0.05% trifluoroacetic acid (TFA); Eluant B, CH_3CN/H_2O 9:1 v/v + 0.05% TFA; gradient 70–100% B in 30 min. The purified fractions were characterized by analytical RP-HPLC on a Phenomenex C18 column (4.6 × 250 mm, 5 μ, 300 Å) using a Dionex (Sunnyvale, CA) system. Eluant A, H_2O/CH_3CN 9:1+ 0.05% TFA; B, CH_3CN/H_2O 9:1 v/v + 0.05% TFA. High-resolution electrospray ionization mass spectrometry (ESI-HRMS) was performed on a PerSeptive Biosystem Mariner instrument (Framingham, MA): $[M+H]^+_{found}$ = 1067.7759, $[M+H]^+_{calcd.}$ = 1067.7132. Analytical HPLC and MS indicate that peptide was obtained at high purity with a yield of 11%.

The para-fluorophenylalanine containing trichogin GA IV ([^{19}F-Phe10]-trichogin GA IV) and the *p*-cyano phenylalanine (PheCN) trichogins were prepared as described in references [81] and [62], respectively. Synthesis of trichogin GA IV-OMe was described in reference [82].

Attenuated total reflection Fourier transform infrared spectroscopy

ATR FTIR polarized spectra were recorded on a Nicolet 670 (Thermo Scientific, Waltham, MA, USA) FTIR spectrometer in the ATR mode, collecting 512 acquisitions for each polarized spectrum, with a 2 cm^{-1} resolution. The sample was prepared by dissolving peptide and 1-palmitoyl-2-oleoyl-*sn*-glycero-3-phosphocholine (POPC, Avanti Polar Lipids, Alabaster, AL) in $CHCl_3$/methanol (1:1 *v*/*v*) at different peptide-to-lipid ratios. An amount of the mixture corresponding to a total lipid quantity of 1 to 1.5 mg was then spread onto a 8 cm x 1 cm x 0.3 cm Ge crystal (reflection angle 45°, 12 reflections on the sample surface) and dried under a gentle argon stream. Organic solvents were completely evaporated by putting the sample under vacuum for two hours. The sample was then hydrated by placing a water-containing vessel into a gas-tight chamber onto the Ge crystal. D_2O was used with trichogin GA IV-OMe, and H_2O with the PheCN labeled peptides. Spectra were acquired every hour for at least six hours. After the first two hours, no changes were detected in the position or intensity of the bands, indicating that the equilibrium was reached. H_2O absorption in the amide I region was subtracted by normalizing a liquid water spectrum to the band in the spectral region around 2125 cm^{-1} [83].

The electric field components of the ATR evanescent field were calculated considering a refractive index n of 4 for Ge and of 1.44 for the lipids [48]. The thick film approximation was adopted, based on the amount of lipids spread on the film: considering an area per lipid of 0.68 nm^2 and a bilayer spacing of 6.4 nm [84], a thickness of more than 2 µm is predicted, to be compared with a calculated penetration depth of 0.4 µm [48].

The order parameter was derived with the following equation [48]:

$$S = \frac{R - \left(\frac{E_X}{E_Y}\right)^2 - \left(\frac{E_Z}{E_Y}\right)^2}{R - \left(\frac{E_X}{E_Y}\right)^2 + 2\left(\frac{E_Z}{E_Y}\right)^2}$$

where *R* is the dichroic ratio (0°/90°)of the peptide amide I band, calculated between 1600 and 1700 cm^{-1}, while the relative amplitudes of the three components of the electric field (E_x, E_y, E_z) are given by $\left(\frac{E_X}{E_Y}\right)^2 = 0.85, \left(\frac{E_Z}{E_Y}\right)^2 = 1.15$ [48]. *S* corresponds to

$$S = \frac{< 3cos^2\alpha > -1}{2} * \frac{< 3cos^2\beta > -1}{2}$$

Here α is the angle between the helix axis and the membrane normal, and β is the angle between the transition dipole of the IR absorption band and the helix axis. For the value of the latter, an angle of 27° has been considered [48].

The correct self-assembly of the lipid multi-bilayer was assessed by measuring the dichroic ratio of the symmetric CH_2 stretching band between 2800 and 2880 cm^{-1}. For all samples, the order parameter was between 0.1 and 0.15; these values are compatible with those obtained for ordered, fully hydrated samples of unsaturated PC lipids [83].

Samples for solid-state NMR spectroscopy

A homogeneous mixture in chloroform of POPC (Avanti Polar Lipids, Alabaster, AL) and ^{19}F-trichogin (peptide/lipid molar ratio 1:8) was prepared. The solution was first dried under a stream of nitrogen gas and thereafter under high vacuum overnight. The mixture was dispersed in 10 mM Tris buffer (pH 7.5) by vortex mixing. The hydrated lipid bilayers were subjected to five rapid freeze-thaw cycles, centrifuged, and concentrated by pelleting in a benchtop centrifuge. After removal of the excess buffer, multilamellar vesicles at a final water concentration of ~50% w/w were obtained.

To calibrate the interactions that occur between ^{19}F spins during the CODEX experiments [85], a 4-^{19}F-2′-nitroacetanilide powder was used. The MAS speed was 15 kHz. A decay constant of 26 ms and an equilibrium value of 0.5 were observed, resulting in the overlap integral value of 100 μs (Fig. 3).

For oriented membrane samples a homogeneous mixture of POPC and peptide was obtained by co-dissolving the membrane components in chloroform. The solution was spread onto ultra-thin cover glasses (8 × 12 mm, Marienfeld, Lauda-Königshofen, Germany), dried first in air or under a stream of nitrogen gas and thereafter under high vacuum overnight. Thereafter, the membranes were equilibrated at 93% relative humidity before the glass slides were stacked on top of each other.

Solid-state NMR spectroscopy

Proton-decoupled ^{31}P solid-state NMR spectra were acquired at 121.577 MHz on a Bruker Avance wide-bore 300 solid-state NMR spectrometer equipped with a commercial (Bruker BioSpin, Rheinstetten, Germany) double-resonance flat-coil probe [86]. A phase-cycled Hahn-echo pulse sequence [87] with a $\pi/2$ pulse of 5 ms, a spectral width of 100 kHz, an echo delay of 40 ms, an acquisition time of 10.2 ms, and a recycle delay of 3 s were used. Spectra were referenced externally to 85% H_3PO_4 at 0 ppm. The temperature was set to 295 K.

Proton-decoupled ^{15}N cross-polarization (CP) spectra were recorded at 76.02 MHz on a Bruker Avance wide bore NMR spectrometer operating at a ^{1}H frequency of 750 MHz using a commercial (Bruker BioSpin, Rheinstetten, Germany) e-free double-resonance flat-coil probe [86] and a cross polarization pulse sequence [54, 88]. The spectral width, acquisition time,

CP contact time, and recycle delay time were 100 kHz, 3.9 ms, 0.4 ms, and 2 s, respectively. The ^{1}H $\pi/2$ pulse and SPINAL-64 heteronuclear decoupling field strengths were 35 kHz [89]. Prior to Fourier transformation an exponential line-broadening of 50 to 200 Hz was applied. $^{15}NH_4Cl$ was used as an external reference and its resonance set to 39.3 ppm [90].

^{19}F MAS solid-state NMR spectra were acquired at 470.4 MHz on an Avance wide-bore 500 NMR spectrometer (Bruker BioSpin, Rheinstetten, Germany) equipped with a triple-resonance MAS 3.2 mm probe that allows simultaneous tuning of the ^{1}H and ^{19}F frequencies on a single channel through a combiner/splitter assembly. The spinning speed was set to 15 kHz. Experiments were conducted at 240 K using cold air (see below). The typical radiofrequency field strength was 70 kHz for ^{19}F and 50 kHz for ^{1}H. The recycle delay was 1.5 s and the CP contact time 0.14 ms. The ^{19}F chemical shifts were referenced to the Teflon ^{19}F signal at -122 ppm.

^{19}F-CODEX experiments were performed as described in references 18, 51. The normalized intensity, S/S_0, was measured as a function of the mixing time until it reached a plateau. Error bars were propagated from the signal/noise ratios of the S_0 and S spectra. The reference experiment (S_0) was conducted by using the same sample but under conditions in which spin diffusion was absent and the signal decay was governed solely by T_2 relaxation. For temperature control, dry air at 223 K was sent from the Bruker cooling unit (BCU Xtreme, Bruker BioSpin, Rheinstetten, Germany) to the MAS probe. To reach 240 K for the membrane samples, the temperature was set to 226 K, since previous calibration measurements showed that 15 kHz MAS adds ~14 K at the level of the sample [18].

ACKNOWLEDGEMENTS

We are most grateful to Prof. Jan Raap for discussion and help with this paper. LS is grateful to the Italian Ministry of Education, Universities and Research, grant PRIN 20157WW5EH and the AIRC, grant IG2016 19171. M.D.Z. and L.S. gratefully acknowledge MIUR (PRIN 20173LBZM2 and 20157WW5EH, respectively) for financial support. BB wishes to thank for the financial contributions of the Agence Nationale de la Recherche (projects membrane DNP 12-BSV5-0012, MemPepSyn 14-CE34-0001-01, InMembrane 15-CE11-0017-01, Biosupramol 17-CE18-0033-3 and the LabEx Chemistry of Complex Systems 10-LABX-0026_CSC), the University of Strasbourg, the CNRS, the *Région Grand-Est (Alsace)* and the RTRA International Center of Frontier Research in Chemistry are gratefully acknowledged. BB is grateful to the *Institut Universitaire de France* for providing additional time to be dedicated to research.

REFERENCES (ok till 52, then changes)

[1] J. L. Lau, M. K. Dunn *Bioorg Med Chem*. **2018**, *26*, 2700-2707.
[2] C. Toniolo, H. E. Brückner *Chem. Biodivers.* **2007**, *4*.
[3] C. Toniolo, H. Brückner, Peptaibiotics: Fungal Peptides Containing α-Dialkyl α-Amino Acids. , Wiley-VCD, Weinheim, Germany, **2009**.
[4] H. Brückner, C. E. Toniolo *Chem. Biodivers.* . **2013**, *10*.
[5] M. De Zotti, B. Biondi, F. Formaggio, C. Toniolo, L. Stella, Y. Park, K. S. Hahm *J Pept Sci*. **2009**, *15*, 615-619.
[6] C. Toniolo, H. e. Brückner, Peptaibiotics, Wiley-VCH, Weinheim, Germany, **2009**.
[7] C. Peggion, F. Formaggio, M. Crisma, R. F. Epand, R. M. Epand, C. Toniolo *J Pept Sci*. **2003**, *9*, 679-689.
[8] M. De Zotti, B. Biondi, C. Peggion, F. Formaggio, Y. Park, K.-S. Hahm, C. Toniolo *Org. Biomol. Chem.* **2012**, *10*, 1285-1299.
[9] R. Tavano, G. Malachin, M. De Zotti, C. Peggion, B. Biondi, F. Forrnaggio, E. Papini *Biochim Biophys Acta*. **2015**, *1848*, 134-144.
[10] B. Leitgeb, A. Szekeres, L. Manczinger, C. Vagvolgyi, L. Kredics *Chem Biodivers.* **2007**, *4*, 1027-1051.
[11] M. S. Sansom *Eur.Biophys.J.* **1993**, *22*, 105-124.
[12] B. Bechinger *J Membrane Biol*. **1997**, *156*, 197-211.
[13] K. Bertelsen, J. M. Pedersen, B. S. Rasmussen, T. Skrydstrup, N. C. Nielsen, T. Vosegaard *J Am.Chem Soc.* **2007**, *129*, 14717-14723.
[14] C. L. North, M. Barranger-Mathys, D. S. Cafiso *Biophys.J.* **1995**, *69*, 2392-2397.
[15] B. Bechinger, D. A. Skladnev, A. Ogrel, X. Li, N. V. Swischewa, T. V. Ovchinnikova, J. D. J. O'Neil, J. Raap *Biochemistry-Us*. **2001**, *40*, 9428-9437.
[16] E. S. Salnikov, M. De Zotti, F. Formaggio, X. Li, C. Toniolo, J. D. O'Neil, J. Raap, S. A. Dzuba, B. Bechinger *J.Phys.Chem.B*. **2009**, *113*, 3034-3042.
[17] E. S. Salnikov, H. Friedrich, X. Li, P. Bertani, S. Reissmann, C. Hertweck, J. D. O'Neil, J. Raap, B. Bechinger *Biophys.J.* **2009**, *96*, 86-100.
[18] E. S. Salnikov, J. Raya, M. De Zotti, E. Zaitseva, C. Peggion, G. Ballano, C. Toniolo, J. Raap, B. Bechinger *Biophys J*. **2016**, *111*, 2450–2459.
[19] E. Salnikov, C. Aisenbrey, V. Vidovic, B. Bechinger *Biochim. Biophys. Acta* **2010**, *1798*, 258-265.
[20] H. W. Huang *Biochimica et Biophysica Acta*. **2006**, *1758*, 1292-1302.
[21] L. Stella, M. Burattini, C. Mazzuca, A. Palleschi, M. Venanzi, I. Coin, C. Peggion, C. Toniolo, B. Pispisa *Chem Biodivers*. **2007**, *4*, 1299-1312.
[22] D. R. Laver *Biophys J*. **1994**, *66*, 355-359.
[23] S. J. Ye, H. C. Li, F. Wei, J. Jasensky, A. P. Boughton, P. Yang, Z. Chen *J Am Chem Soc*. **2012**, *134*, 6237-6243.
[24] K. He, S. J. Ludtke, W. T. Heller, H. W. Huang *Biophys.J.* **1996**, *71*, 2669-2679.
[25] C. Auvin-Guette, S. Rebuffat, Y. Prigent, B. Bodo *J. Am. Chem. Soc.* **1992**, *114*, 2170–2172.
[26] C. Heuber, F. Formaggio, C. Baldini, C. Toniolo, K. Muller *Chem Biodivers*. **2007**, *4*, 1200-1218.
[27] E. S. Salnikov, D. A. Erilov, A. D. Milov, Y. D. Tsvetkov, C. Peggion, F. Formaggio, C. Toniolo, J. Raap, S. A. Dzuba *Biophys J*. **2006**, *91*, 1532-1540.
[28] E. F. Afanasyeva, V. N. Syryamina, M. De Zotti, F. Formaggio, C. Toniolo, S. A. Dzuba *Bba-Biomembranes*. **2019**, *1862*, 524-531.
[29] V. N. Syryamina, M. De Zotti, C. Peggion, F. Formaggio, C. Toniolo, J. Raap, S. A. Dzuba *Journal of Physical Chemistry B*. **2012**, *116*, 5653-5660.

[30] M. Bortolus, A. Dalzini, A. L. Maniero, G. Panighel, A. Siano, C. Toniolo, M. De Zotti, F. Formaggio *Biopolymers*. **2017**, *108*.
[31] R. F. Epand, R. M. Epand, V. Monaco, S. Stoia, F. Formaggio, M. Crisma, C. Toniolo *European Journal of Biochemistry*. **1999**, *266*, 1021-1028.
[32] L. Stella, C. Mazzuca, M. Venanzi, A. Palleschi, M. Didone, F. Formaggio, C. Toniolo, B. Pispisa *Biophys J*. **2004**, *86*, 936-945.
[33] C. Mazzuca, L. Stella, M. Venanzi, F. Formaggio, C. Toniolo, B. Pispisa *Biophys J*. **2005**, *88*, 3411-3421.
[34] E. Gatto, C. Mazzuca, L. Stella, M. Venanzi, C. Toniolo, B. Pispisa *J Phys Chem B*. **2006**, *110*, 22813-22818.
[35] C. Mazzuca, B. Orioni, M. Coletta, F. Formaggio, C. Toniolo, G. Maulucci, M. De Spirito, B. Pispisa, M. Venanzi, L. Stella *Biophys J*. **2010**, *99*, 1791-1800.
[36] C. Toniolo, C. Peggion, M. Crisma, F. Formaggio, X. Shui, D. S. Eggleston *Nat Struct Biol*. **1994**, *1*, 908-914.
[37] M. Smetanin, S. Sek, F. Maran, J. Lipkowski *Bba-Biomembranes*. **2014**, *1838*, 3130-3136.
[38] S. Bobone, Y. Gerelli, M. De Zotti, G. Bocchinfuso, A. Farrotti, B. Orioni, F. Sebastiani, E. Latter, J. Penfold, R. Senesi, F. Formaggio, A. Palleschi, C. Toniolo, G. Fragneto, L. Stella *Bba-Biomembranes*. **2013**, *1828*, 1013-1024.
[39] S. Smeazzetto, M. De Zotti, M. R. Moncelli *Electrochem Commun*. **2011**, *13*, 834-836.
[40] L. Becucci, F. Maran, R. Guidelli *Biochim Biophys Acta*. **2012**, *1818*, 1656-1662.
[41] S. Iftemi, M. De Zotti, F. Formaggio, C. Toniolo, L. Stella, T. Luchian *Chem Biodivers*. **2014**, *11*, 1069-1077.
[42] G. Bocchinfuso, A. Palleschi, B. Orioni, G. Grande, F. Formaggio, C. Toniolo, Y. Park, K. S. Hahm, L. Stella *J Pept Sci*. **2009**, *15*, 550-558.
[43] M. De Zotti, B. Biondi, Y. Park, K. S. Hahm, M. Crisma, C. Toniolo, F. Formaggio *Amino Acids*. **2012**, *43*, 1761-1777.
[44] T. N. Kropacheva, J. Raap *Biochim Biophys Acta*. **2002**, *1567*, 193-203.
[45] L. Stella, S. Bobone, G. Bocchinfuso, A. Palleschi, J. Y. Kim, Y. Park, K. S. Hahm *J Pept Sci*. **2010**, *16*, 137-137.
[46] N. Vedovato, G. Rispoli *Eur.Biophys J*. **2007**, *36*, 771-778.
[47] B. Bechinger, C. Sizun *Concepts in Magnetic Resonance*. **2003**, *18A*, 130 -145
[48] E. Goormaghtigh, V. Raussens, J. M. Ruysschaert *Biochimica et Biophysica Acta - Reviews on Biomembranes*. **1999**, *1422*, 105-185.
[49] B. Bechinger, J. M. Ruysschaert, E. Goormaghtigh *Biophys.J.* **1999**, *76*, 552-563.
[50] E. R. deAzevedo, W. G. Hu, T. J. Bonagamba, K. Schmidt-Rohr *J Am Chem Soc*. **1999**, *121*, 8411-8412.
[51] W. Luo, M. Hong *J. Am. Chem. Soc.* **2006**, *128*, 7242-7251.
[52] M. L. Gilchrist, Jr., K. Monde, Y. Tomita, T. Iwashita, K. Nakanishi, A. E. McDermott *J Magn Reson*. **2001**, *152*, 1-6.
[53] B. Bechinger, E. S. Salnikov *Chem Phys Lipids*. **2012**, *165*, 282-301.
[54] C. Aisenbrey, M. Michalek, E. S. Salnikov, B. Bechinger in *Solid-state NMR approaches to study protein structure and protein-lipid interactions, Vol.* (Ed. J. H. Kleinschmidt), Springer, New York, **2013**, pp.357-387.
[55] J. Wolf, C. Aisenbrey, N. Harmouche, J. Raya, P. Bertani, N. Voievoda, R. Süss, B. Bechinger *Biophys J*. **2017**, *113*, 1290-1300.
[56] C. Kim, J. Spano, E. K. Park, S. Wi *Biochim. Biophys. Acta*. **2009**, *1788*, 1482-1496.
[57] R. M. Verly, C. M. de Moraes, J. M. Resende, C. Aisenbrey, M. P. Bemquemer, D. Pilo-Veloso, A. P. Valente, F. C. Alemida, B. Bechinger *Biophys.J.* **2009**, *96*, 2194-2203.
[58] P. Braun, G. von Heijne *Biochemistry-Us*. **1999**, *38*, 9778-9782.
[59] E. S. Salnikov, A. J. Mason, B. Bechinger *Biochimie*. **2009**, *91*, 734-743.

[60] V. N. Syryamina, N. P. Isaev, C. Peggion, F. Formaggio, C. Toniolo, J. Raap, S. A. Dzuba *Journal of Physical Chemistry B*. **2010**, *114*, 12277-12283.
[61] S. Bobone, M. De Zotti, A. Bortolotti, B. Biondi, G. Ballano, A. Palleschi, C. Toniolo, F. Formaggio, L. Stella *Biopolymers*. **2015**, *104*, 521-532.
[62] M. De Zotti, S. Bobone, A. Bortolotti, E. Longo, B. Biondi, C. Peggion, F. Formaggio, C. Toniolo, A. Dalla Bona, B. Kaptein, L. Stella *Chem Biodivers*. **2015**, *12*, 513-527.
[63] S. A. Tatulian *Biochemistry-Us*. **2003**, *42*, 11898-11907.
[64] A. D. Milov, Y. D. Tsvetkov, F. Formaggio, M. Crisma, C. Toniolo, J. Raap *J Pept.Sci*. **2003**, *9*, 690-700.
[65] E. Salnikov, B. Bechinger *Biophysical J.* . **2011**, *100*, 1473-1480.
[66] B. Perrone, A. J. Miles, E. S. Salnikov, B. Wallace, B. Bechinger *Eur. Biophys. J.* . **2014**, *43*, 499-507.
[67] U. S. Sudheendra, B. Bechinger *Biochemistry-Us*. **2005**, *44*, 12120-12127.
[68] M. Bortolus, A. Dalzini, C. Toniolo, K. S. Hahm, A. L. Maniero *J Pept Sci*. **2014**, *20*, 517-525.
[69] T. C. B. Vogt, P. Ducarme, S. Schinzel, R. Brasseur, B. Bechinger *Biophys.J.* **2000**, *79*, 2644-2656.
[70] A. J. Mason, P. Bertani, G. Moulay, A. Marquette, B. Perrone, A. F. Drake, A. Kichler, B. Bechinger *Biochemistry-Us*. **2007**, *46*, 15175-15187.
[71] J. M. Resende, C. M. Moraes, V. H. D. O. Munhoz, C. Aisenbrey, R. M. Verly, P. Bertani, A. Cesar, D. Pilo-Veloso, B. Bechinger *Proc.Natl.Acad.Sci.U.S.A*. **2009**, *106*, 16639-16644.
[72] C. Aisenbrey, C. Sizun, J. Koch, M. Herget, U. Abele, B. Bechinger, R. Tampe *The Journal of biological chemistry*. **2006**, *281*, 30365-30372.
[73] A. D. Milov, Y. D. Tsvetkov, F. Formaggio, S. Oancea, C. Toniolo, J. Raap *J.Phys.Chem.B*. **2003**, *107*, 13719-13727.
[74] A. D. Milov, A. G. Mar'yasov, R. I. Samoilova, Y. D. Tsvetkov, J. Raap, V. Monaco, F. Formaggio, M. Crisma, C. Toniolo *Dokl.Biochem.* **2000**, *370*, 8-11.
[75] A. Dalzini, C. Bergamini, B. Biondi, M. De Zotti, G. Panighel, R. Fato, C. Peggion, M. Bortolus, A. L. Maniero *Sci Rep*. **2016**, *6*, 24000.
[76] S. A. Dzuba, J. Raap *Chem Biodivers*. **2013**, *10*, 864-875.
[77] M. A. Lemmon, H. R. Treutlein, P. D. Adams, A. T. Brunger, D. M. Engelman *Nature Structural Biology*. **1994**, *1*, 157-163.
[78] D. Sengupta, R. N. Behera, J. C. Smith, G. M. Ullmann *Structure*. **2005**, *13*, 849-855.
[79] C. Aisenbrey, A. Marquette, B. Bechinger in *The Mechanisms of Action of Cationic Antimicrobial Peptides Refined by Novel Concepts from Biophysical Investigations, Vol. 1117* (Ed. K. Matsuzaki), Springer Nature, Singapore, **2019**, pp.33-64.
[80] B. Bechinger *J. Peptide Sci.* **2015**, *21*, 346-355
[81] C. Peggion, B. Biondi, C. Battistella, M. De Zotti, S. Oancea, F. Formaggio, C. Toniolo *Chem. Biodivers.* **2013**, *10*, 904-919.
[82] C. Toniolo, M. Crisma, F. Formaggio, C. Peggion, V. Monaco, C. Goulard, S. Rebuffat, B. Bodo *J Am Chem Soc*. **1996**, *118*, 4952-4958.
[83] L. K. Tamm, S. A. Tatulian *Q Rev Biophys JID - 0144032*. **1997**, *30*, 365-429.
[84] N. Kucerka, S. Tristram-Nagle, J. F. Nagle *J Membr Biol*. **2005**, *208*, 193-202.
[85] W. B. Luo, R. Mani, M. Hong *Journal of Physical Chemistry B*. **2007**, *111*, 10825-10832.
[86] B. Bechinger, S. J. Opella *J.Magn.Reson.* **1991**, *95*, 585-588.
[87] M. Rance, R. A. Byrd *Journal of Magnetic Resonance*. **1983**, *52*, 221-240.
[88] A. Pines, M. G. Gibby, J. S. Waugh *J.Chem.Phys.* **1973**, *59*, 569-590.
[89] B. M. Fung, A. K. Khitrin, K. Ermolaev *J. Magn. Reson.* **2000**, *142*, 97-101.
[90] P. Bertani, J. Raya, B. Bechinger *Solid-state NMR spec.* . **2014**, *61-62*, 15-18